Sensitivity of neural-hemodynamic coupling to alterations in cerebral blood flow during hypercapnia

Theodore J. Huppert
University of Pittsburgh
Department of Radiology
200 Lothrop Street
Pittsburgh, Pennsylvania 15213
and
Massachusetts General Hospital
Athinoula A. Martinos Center for Biomedical Imaging
Charlestown, Massachusetts 02129
E-mail: huppertt@upmc.edu

Phill B. Jones
Massachusetts General Hospital
Athinoula A. Martinos Center for Biomedical Imaging
Charlestown, Massachusetts 02129

Anna Devor
Massachusetts General Hospital
Athinoula A. Martinos Center for Biomedical Imaging
Charlestown, Massachusetts 02129
and
University of California San Diego
Department of Neurosciences
9500 Gilman Drive 0662
La Jolla, California 92093

Andrew K. Dunn
University of Texas
Biomedical Engineering Department
1 University Station, C0800
Austin, Texas 78712

Ivan C. Teng
University of California San Diego
Neurosciences
9500 Gilman Drive 0662
La Jolla, California 92093

Anders M. Dale
University of California, San Diego
Department of Neurosciences
9500 Gilman Drive 0662
La Jolla, California 92093
and
University of California, San Diego
Department of Radiology
9500 Gilman Drive, MC 0657
La Jolla, California 92093

David A. Boas
Massachusetts General Hospital
Athinoula A. Martinos Center for Biomedical Imaging
Charlestown, Massachusetts 02129
and
Harvard Medical School
Massachusetts General Hospital
Department of Radiology
55 Fruit Street
Boston, Massachusetts 02114

Abstract. The relationship between measurements of cerebral blood oxygenation and neuronal activity is highly complex and depends on both neurovascular and neurometabolic biological coupling. While measurements of blood oxygenation changes via optical and MRI techniques have been developed to map functional brain activity, there is evidence that the specific characteristics of these signals are sensitive to the underlying vascular physiology and structure of the brain. Since baseline blood flow and oxygen saturation may vary between sessions and across subjects, functional blood oxygenation changes may be a less reliable indicator of brain activity in comparison to blood flow and metabolic changes. In this work, we use a biomechanical model to examine the relationships between neural, vascular, metabolic, and hemodynamic responses to parametric whisker stimulation under both normal and hypercapnic conditions in a rat model. We find that the relationship between neural activity and oxy- and deoxyhemoglobin changes is sensitive to hypercapnia-induced changes in baseline cerebral blood flow. In contrast, the underlying relationships between evoked neural activity, blood flow, and model-estimated oxygen metabolism changes are unchanged by the hypercapnic challenge. We conclude that evoked changes in blood flow and cerebral oxygen metabolism are more closely associated with underlying evoked neuronal responses. [DOI: 10.1117/1.3210779]

Keywords: neural-hemodynamic coupling; hypercapnia; cerebral blood flow.

Paper 08415RR received Dec. 3, 2008; revised manuscript received Jun. 29, 2009; accepted for publication Jun. 30, 2009; published online Aug. 31, 2009.

1 Introduction

During brain function, an increase in underlying neuronal activity evokes an elevation in the energetic load on the brain. To maintain homeostasis, these increases in neuronal activity must be coupled to both regional increases in glycolytic metabolism and increases in cerebral blood flow. These relationships are termed the neurometabolic and neurovascular pathways respectively. Since the net balance between oxygen delivery and oxygen utilization depends on the influences of

Address all correspondence to: Theodore J. Huppert, Ph.D., Department of Radiology, University of Pittsburgh, Pittsburgh, PA 15213. Tel: 412-647-9700; Fax: 412-647-9800; E-mail: huppertt@upmc.edu

1083-3668/2009/14(4)/044038/16/$25.00 © 2009 SPIE

both these metabolic and vascular responses, there typically exists an ambiguity in the interpretation of the overall blood oxygenation changes as measured by neuroimaging techniques such as intrinsic optical imaging[1–4] and functional magnetic resonance imaging.[5,6]

The interpretation of optical or fMRI measurements requires consideration of both the biochemical and biomechanical properties of the brain. Although originating from both microscopic level coupling between the neurons and blood vessels (termed neurovascular coupling) and through cellular energy metabolism in response to neuronal energetic demand (termed neurometabolic coupling), changes in overall blood oxygenation or oxy- and deoxyhemoglobin also depend on the properties of the underlying cerebral vascular structures and baseline vascular physiology. For purposes here, the overall response in blood oxygenation as measured by optical or fMRI is termed the hemodynamic response, while the indirect relationship between the neurons and these blood oxygenation changes is termed neurohemodynamic coupling and is the result of both underlying neurometabolic and neurovascular effects.

Blood oxygenation changes during typical brain activity are predominantly the result of the washout (or displacement) of deoxyhemoglobin by an increase in the supply of highly oxygenated (arterial) blood in conjunction with increases in blood volume. To a much lesser extent, the conversion of oxyhemoglobin to deoxyhemoglobin by oxidative metabolism also effects blood oxygenation. However, generally, cerebral blood flow increases are around two- to four-fold larger than these oxygen metabolism changes, which produce the typical hyperemic evoked hemodynamic response comprising an overall increase in blood oxygenation levels. Since this washout effect depends on the amount of deoxyhemoglobin in the blood vessels at baseline, the evoked hemodynamic response to a given stimulus is altered if baseline oxygenation levels are varied.

In recent years, there has been increasing experimental evidence that the characteristics of the evoked hemodynamic responses are sensitive to variability in this baseline vascular physiology. As cases in point, several recent studies have demonstrated that both the magnitude and temporal dynamics of evoked blood oxygen level dependent (BOLD) MRI and optical signals can be altered by the experimental manipulation of baseline perfusion using varied levels of inspired carbon dioxide or oxygen,[7,8] or pharmacological agents.[9–11] Although a number of studies have investigated the empirical relationships between electrophysiological changes and oxygenation changes available from optical measurements of oxy- and deoxyhemoglobin[8,12,13] or the BOLD signal,[14–16] only a few studies have examined the generality of neurovascular relationships across varied levels of background physiology.[8,17] To further quantify the relationships between the BOLD or optical signals and underlying neural activity, we need to consider the influences of both the metabolic and vascular factors that contribute to net blood oxygenation and the potential confounds of variability in vascular physiology (reviewed in (Refs. 18 and 19). Because of the role that the physical and biomechanical structure of the vascular network places in defining evoked hemodynamic changes (e.g., Ref. 20), we hypothesize that the relationship between neural and blood oxygenation changes may be less repeatable across experiment conditions than the relationships between neuronal and metabolic or vascular responses.

To test this hypothesis, we designed an experiment to examine how the relationships between neural, vascular, metabolic, and blood oxygenation signals were changed, or alternatively if these were unchanged, by experimentally manipulating the vascular physiology through hypercapnia. Hypercapnia induces an increase in blood flow and decrease in the oxygen extraction fraction, and thus alters the vascular physiology of the brain that dictates the behavior of functionally evoked changes in oxy- and deoxyhemoglobin. Although the baseline dependence of these blood oxygenation changes had been previously demonstrated qualitatively, we sought to determine if these effects could be quantitatively explained by a model-based approach to account for the differences in baseline physiology and associated model parameters between the normal and hypercapnic states. In particular, we used a vascular model-based analysis as introduced in Ref. 21 to infer the underlying changes in arterial resistance (causing blood flow changes) and oxygen metabolism changes. This approach allowed us to predict the underlying physiological changes as hidden states (not directly observable values) based on their relationship to experimental recordings of blood flow, volume, and oxygenation changes from optical imaging. We looked at the relationship of these underlying physiological signals and neural activity. This model also allowed us to look at how the parameters of the model—e.g., the model constants such as the vascular transit time that define the relationships between the time-varying physiological measurements—differed between the normal and hypercapnic conditions, and thus, to examine if the observed differences in the time courses of the evoked responses under these two baseline conditions could be predicted from the value of these parameters. For example, hypercapnia is expected to increase baseline blood flow, which would change the model parameters defining increased baseline oxygen saturation, increased baseline blood volume, and decreased vascular transit time. The effect of these changes in the model parameters on the experimental measurements can be simulated and compared to experimental measurements. This allows us to address the question of whether changes in the evoked responses under hypercapnia are due to changes in baseline physiology, differences in neural activity, or differences in the underlying neurovascular and neurometabolic relationships.

In this study, we used invasive experimental optical techniques to measure blood oxygenation and blood flow changes, and simultaneously made recordings of neuronal electrical activity under different levels of expired CO_2. We measured evoked changes across multiple stimulus conditions within the whisker barrel cortex of a rat. We then used a multicompartment vascular model described in Ref. 21 to explore how variations in baseline blood flow and volume can alter the magnitude and temporal characteristics of the evoked hemodynamic response. This model allowed us to test whether the differences we observed in evoked responses between the normal and hypercapnic conditions could be attributed to biomechanical causes due to the changes in baseline blood oxygenation, blood volume and flow, and vascular transit time.

Using our vascular model, we investigated the coupling between the measured neuronal activity, the hemodynamic responses, and the underlying blood flow and oxygen metabo-

lism changes. We found significant linear correlation between all of these coupling relationships. However, when baseline flow was changed by hypercapnia, the relationship between the neural and blood oxygenation signals (oxy- and deoxyhemoglobin) also changed, whereas the neurovascular and neurometabolic coupling relationships were the same. Thus, while under both the normal and hypercapnia conditions, a linear relationship between neural activity and overall blood oxygenation was observed. The nature of this relationship (e.g., slope) differed according to baseline physiology. This result confirms our hypothesis that the relationship between hemodynamic changes and neuronal activity depends on the baseline conditions, whereas neurovascular and neurometabolic coupling are insensitive to these baseline effects and thus more revealing of the underlying neural activity in the brain. Furthermore, we find that the hypercapnia-induced differences that were observed in the blood oxygenation responses are consistent with the mechanical effects expected from the changes in the model parameters based on measured differences in blood flow, volume, and oxygen saturation between normal and hypercapnic states. We conclude that blood flow and $CMRO_2$ changes remain closely associated with underlying neuronal activity across differing levels of baseline physiology, and thus may be more reliable for longitudinal studies of brain activity in comparison to oxyhemoglobin, deoxyhemoglobin, and BOLD MRI signal changes.

2 Experimental Methods

2.1 *Animal Preparation*

The Massachusetts General Hospital Subcommittee on Research Animal Care approved all experimental procedures. Male Sprague-Dawley rats ($n=7$; 250 to 350 g) were anesthetized with halothane (1.5 to 0.7%) in a mixture of 70% medical air and 30% oxygen for surgery. Glycopyrrolate (0.5 mg/kg, i.m.) was administered 10 min before the initiation of anesthesia. During surgery, a tracheotomy was performed and cannulas were inserted in the femoral artery and vein. All incisions were infiltrated with 2% lidocaine. Following tracheotomy, rats were mechanically ventilated. Ventilation parameters were adjusted to maintain Pa_{CO_2} between 35- and 45-mm Hg, Pa_{O_2} between 140- and 180-mm Hg, and pH between 7.35 and 7.45. The animal was then fixed in a stereotaxic frame. An area of skull overlying the primary somatosensory cortex was exposed and thinned with a dental burr until soft and transparent ($\sim 100\ \mu$m). A well of dental acrylic was built around the border of the thinned skull, which then was filled with saline. For simultaneous electrophysiological recordings using single metal microelectrodes, a small hole was made in the thinned skull and dura mater centered on the maximal evoked response, as determined by optical imaging, and the recording electrode was inserted at depth of 400 μm (cortical layer 3). Following the surgery, halothane was discontinued, and anesthesia was maintained with 50-mg/kg intravenous bolus of α-chloralose, followed by continuous intravenous infusion at $40\text{-mg}*\text{kg}^{-1}*\text{h}^{-1}$. Heart rate, electrocardiogram (ECG), body temperature, and blood pressure were monitored continuously during the experiment. Body temperature was maintained at $37.0\ ^\circ\text{C} \pm 0.5\ ^\circ\text{C}$ with a homeothermic blanket (Harvard Apparatus, Holliston, Massachusetts). Blood samples (0.1 ml) were withdrawn for blood gas measurements.

2.2 *Hypercapnia Procedure*

Hypercapnia was induced by adding CO_2 (2.5% or 5%) to the inspired gas mixture. Five minutes were allowed for transition between normocapnia and hypercapnia. In four of the seven animals, optical signals were reliably recorded during this transition period, which was used to estimate the blood flow and hemoglobin changes induced by the hypercapnia challenge.

Because of a high degree of variability in the effect of hypercapnia on individual rats, more statistical power could be obtained by grouping the two conditions of hypercapnia (2.5 and 5%) and performing all comparisons directly between the normal and mixed hypercapnia states, which still allowed us to test if neurohemodynamic coupling varied with baseline state. Of the seven animals used in this study, four experienced 2.5% CO_2 and the remaining three animals received 5% CO_2. Because of variability in the hypercapnic response, we did not observe significant differences between the magnitudes of the hemodynamic or neural responses under 2.5 and 5% CO_2 states.

2.3 *Stimulation Paradigm*

The stimulus consisted of a 2-sec-long train of whisker deflections at 8 Hz during both normal and hypercapnic states. A single whisker (D1) was deflected by a computer-controlled piezoelectric stimulator. Single whiskers were deflected at 8 Hz for a 2-s duration. We used varying deflection amplitudes (from 1 to 9) corresponding to the angular velocity increased from 230 deg/s (vertical displacement of 240 μm, condition 1) to 969 deg/s (vertical displacement of 1200 μm, condition 9), with equal amplitude increments. Stimuli were presented using a rapid, randomized event-related paradigm using 3-sec interstimulus interval and 25% blanks.[22]

2.4 *Description of Optical System and Analysis*

Blood oxygenation and flow was measured using simultaneous multiwavelength spectroscopic imaging of total hemoglobin concentration and oxygenation and laser speckle imaging of blood flow.[23] The cortex was illuminated by a filtered tungsten-halogen lamp (10-nm bandpass filters centered at wavelengths of 560, 570, 580, 590, 600, and 610 nm). Images were acquired onto a cooled 12-bit charge-coupled device (CCD) camera at a frame rate of 12 to 15 Hz. Spectral images for each trial were divided by the baseline image, calculated as an average of images within 1 sec before the stimulus onset. The modified Beer-Lambert law was used to convert these spectral images into images of relative oxy- and deoxyhemoglobin concentration changes with differential path length factors used to account for the individual optical pathlengths at each wavelength as described in Ref. 24. Blood flow was imaged simultaneously using a cooled 8-bit CCD camera at a frame rate of 200 Hz. Images of relative cerebral blood flow (CBF) changes were determined by calculating the changes in the speckle contrast in a series of temporally down-sampled (factor of 10) laser speckle images. The speckle contrast was calculated as the ratio of the standard

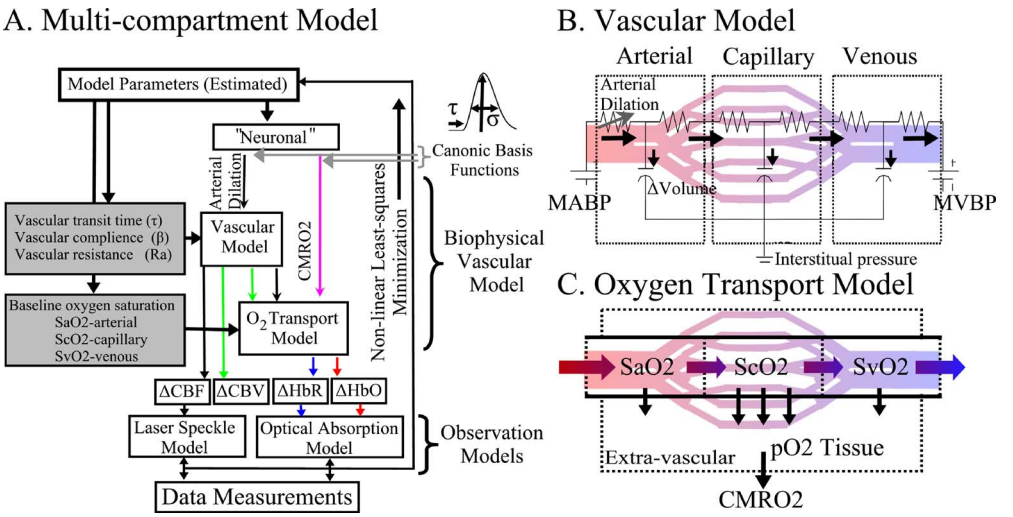

Fig. 1 Schematic overview of the multicompartment forward model. The multicompartment model of the vascular network describes the temporal evolution of the evoked hemodynamic states as a result of neuronally linked changes in the resistance of arterial smooth muscle and changes in the oxygen consumption ($CMRO_2$) in the extravascular space. In (a), we show an overview of the entire vascular model consisting of the vascular, oxygen transport, and observation models.[21] (b) and (c), show schematics of the vascular and oxygen transport components of the model.

deviation to the mean pixel intensities $\sqrt{\langle I^2\rangle}/\langle I\rangle$ over a 5 $\times$5 pixel spatial sliding window.[25] Speckle contrast images for each trial were divided by the baseline image, calculated as an average of images within 1 s before the stimulus onset. Averaged across trials images were converted to relative blood flow as described in Dunn et al.[26] Regions of interest were defined by first manually selecting a region enclosing the barrel cortex corresponding to the stimulated whisker, as was determined by electrophysiological mapping. Signals were then averaged from all pixels within this region whose peak amplitude was greater than half the respective maximal responses in both the flow and oxyhemoglobin images. For more details on the region-of-interest selection, see Dunn et al.[26] To increase statistical power and reduce intersubject effects, the group average of the seven animals was calculated after normalizing to the amplitude of the ninth condition (the largest deflection amplitude) of the normocapnia response.

2.5 *Description of Electrophysiology Recordings and Analysis*

Electrophysiological recordings were made using single metal microelectrodes [FHC (Bowdoinham, Maine), 5 to 7 MΩ]. The recorded potential was amplified and filtered into two signals: a low-frequency part (0.1 to 500 Hz, sampled at 2 kHz with 16 bits) and a high-frequency part (150 to 5000 Hz, sampled at 20 kHz with 12 bits; see Ref. 27 for details). The low-frequency part is referred to as the local field potential (LFP). The high-frequency part was further filtered digitally between 750 and 5000 Hz using a zero phase-shift second-order Butterworth filter, and then rectified along the time axis to provide the multiple unit activity (MUA). Finally, the MUA data were smoothed along the time axis using a Gaussian kernel of 1 msec full width at e^{-1} of peak amplitude. The LFP and MUA responses were again normalized to the peak magnitude of the normocapnia (ninth condition) before group averaging.

We examined both the peak magnitude and the integrated amplitude of the LFP and MUA responses. The peak magnitudes were defined as the magnitude of the first evoked response in the stimulus train. Integrated electrical response (denoted by Σ in this work) was defined as the square root of the sum of the squared amplitudes for the entire two-second train of responses.

3 Numerical Analysis Methods

3.1 *Description of Multicompartment Model*

We used a multicompartment balloon model[21] to characterize the vascular and metabolic responses driving the observed blood flow, volume, and oxygenation responses, and to examine the biomechanical effects of the hypercapnia-induced change in baseline blood flow, volume, and oxygen saturation on the evoked signals. This model is based on a bottom-up framework, as diagramed in Fig. 1, and is used to forward model expected hemodynamic signals based on a set of dynamic input states (arterial resistance and relative $CMRO_2$ changes) and a set of baseline and structurally related model parameters listed in Table 1. The model is based on a set of differential equations that describe the biomechanical response of the arterial, capillary, and venous blood vessels to changes in arterial resistance (e.g., dilation of the arteries in response to neurovascular coupling). Based on the blood flow change predicted from the vascular model component and a second model input describing oxygen consumption (neurometabolic coupling), the oxygen content of the blood vessels is also modeled using the principles of mass balance. Thus, our model has several static model parameters describing features such as baseline blood oxygenation and two dynamic inputs; the evoked change in arterial dilation and oxygen metabolism ($CMRO_2$), which are used to predict the changes in measurable blood flow, volume, and oxy/deoxyhemoglobin. A model of the laser speckle and optical spectroscopy measurement processes connects the underlying

Table 1 Biomechanical model parameters. The vascular forward model of the dynamics of evoked hemodynamic changes depends on several mechanical and baseline physiological parameters and were fully described in Refs. 21 and 28. These parameters, which affect both the temporal dynamics and magnitudes of evoked physiological signals, can be estimated from the model-based curve fitting of hemodynamic measurements, as described earlier. Six additional model parameters per stimulus condition define the combined arterial resistance and $CMRO_2$ changes as described in the text.

Parameter	Symbol	Description	Range of parameter in model	
Initial arterial resistance	Ra_o	Fraction of total vascular resistance attributed to the arterial compartment.	20 to 90%	Ref. 41
Vascular compliance parameter	β	The vascular compliance parameter determines the relationship of evoked flow and volume changes.	1 to 4	Ref. 42
Vascular transit time	τ	Vascular transit time through arterial to venous compartment. Defined as the ratio of baseline volume and flow.	0.5 to 4 s	Ref. 43
Pial venous transit time	τ_{pial}	Transit time of pial venous compartment.	0 to 4 s	
Total hemoglobin concentration	THC	Amount of baseline total hemoglobin. Used to scale normalized values from model to optical measurements.	40 to 140 μM	Ref. 44
Arteriole saturation	S_AO_2		90 to 100%	
Capillary saturation	S_CO_2	Fraction of oxygenated hemoglobin in each vascular compartment.	60 to 90%	Ref. 45
Venous saturation	S_VO_2		55 to 89%	

vascular model and the actual experimental measurements by describing the biophysics of the observation processes that give rise to these measurements. This model includes an estimate of the measurement error, which is used to weight the contributions from each measurement. We represent these measurements as the sum of the changes in oxy/deoxyhemoglobin and mean of blood flow over the vascular segments.

The model is fit to experimental data (further detailed later) to estimate both the parameters and the inputs that best describe the set of measured responses. The detailed mathematical description of this model and the model inversion routine is detailed in Refs. 21 and 28. Further details about parameter estimation, identifiablity, and derivation of the algorithms used in this model can be found in Ref. 28 (specifically see Appendix 4).

3.2 *Vascular and Metabolic Changes*

In the model, the $CMRO_2$ and arterial resistance states are described by a set of parameterized nonlinear canonical functions as described in Refs. 21 and 28. First, the dilation of the arteries is defined using a canonical Gaussian-based temporal basis function with variable timing parameters (time-to-peak τ_{peak}; temporal width σ; and maximum fractional displacement $\Delta\%^{max}R_A$,

$$1-\frac{R_A(t)}{R_A(t=0)}=\Delta_{\%}^{max}R_A\frac{H(t)}{\sqrt{\sigma^2\pi}}\exp\left[\frac{-(t-\tau_{peak})^2}{\sigma^2}\right]. \quad (1)$$

The function $H(t)$ represents the heavy-side hat function. The parameters defining the arterial resistance function were estimated within the range of 0 to 6 sec for both the time-to-peak and temporal width, and 0 to 10% for the value of the maximal resistance change. A gamma-variant functional form with variable timing and amplitude describes $CMRO_2$ changes similar to the method describing the arterial resistance function.

$$\frac{CMRO_2(t)}{CMRO_2(t=0)}-1=\Delta_{\%}^{max}CMRO_2\frac{H(t-\tau_{offset})(t-\tau_{offset})^2}{\sigma^2\exp(-1)}\cdot\exp\left[\frac{-(t-\tau_{offset})^2}{\sigma^2}\right]. \quad (2)$$

Our model was used to estimate the values of the parameters defining the $CMRO_2$ function within the range of 0 to 2 sec for the response onset time, 0 to 6 sec for the temporal width, and 0 to 10% for the value of the maximal $CMRO_2$ change. The choice of these two basis functions is detailed in Ref. 21. Arguably, the ranges used for these parameters were liberal,

as we expect resistance and metabolism changes to be much smaller than the allowed 10%.

3.3 *Vascular Inverse Model*

Cerebral oxygen metabolism was estimated from a curve fitting of the multimodal observations. We use a nonlinear, Levenberg-Marquardt algorithm[29] implemented in Matlab to estimate all model parameters (Table 1). A differential time step of 2 ms was utilized for the update of the vascular and oxygen transport models. Smaller time steps were also tested to verify that the results were independent of this choice. The different multimodal measurements were combined using a weighted least-squares cost function. For each measurement type, these weights were calculated from the variance in the estimate of the hemodynamic responses across multiple trials. A prior physiological range of values based on the literature is used to constrain the values for each parameter as given in Table 1. The model we used in this work is identical to the one described in Ref. 21. In our fitting routine, we simultaneously considered the data from all nine stimulus conditions. A single set of biomechanical parameters (listed in Table 1) and nine independent $CMRO_2$ and arterial resistance responses are used to model the nine parametric hemodynamic responses. The normal and hypercapnic measurements are independently analyzed such that the results from the two models could be compared without potentially biasing the results.

Since we are analyzing all nine response conditions simultaneously, the model has eight baseline-related parameters and 54 (six parameters per nine conditions) total parameters, which are simultaneously fit to 27 independent time-course recordings (oxy/deoxyhemoglobin and blood flow for each of the nine conditions). Each of these time courses can conservatively be estimated to have at least three independent degrees of freedom—amplitude, time-to-peak/onset (first temporal moment), and temporal width (second temporal moment)—thus providing some expectation that all parameters can be estimated by the modeling fitting procedure. For further treatment of the behavior of this model, see Ref. 28. To estimate the confidence bounds for each of the model parameters, we performed a Markov chain Monte Carlo sampling of the parameter space and estimated the 95% confidence intervals for each parameter.

3.4 *Relationships of Model Parameters to Baseline Physiology*

Many of the parameters in our model can be estimated based on the relative timing between components of the hemodynamic response. For example, the temporal lag between the time courses of oxy- and deoxyhemoglobin is sensitive to the value of the mean vascular transit. Many of the biomechanical parameters within our model, which are estimated based on the temporal dynamics and relative magnitudes of the evoked signals, can be related to the values of baseline blood flow, volume, and $CMRO_2$, as detailed in Refs. 21 and 28. For instance, the mean transit time is physiologically defined as the ratio of baseline blood volume and flow. Likewise, the ratio of the micromolar total-hemoglobin concentration changes and relative blood volume changes is used in the model as an estimated calibration parameter equal to baseline total-hemoglobin concentrations. The values estimated for the baseline total-hemoglobin concentration (THC) and the mean vascular transit time (τ) are sufficient to estimate the value of baseline blood flow using the steady-state relationship,

$$\mathrm{CBF}_0 = \frac{\mathrm{THC}\,\mathrm{MW}_{\mathrm{Hb}}}{\mathrm{HGB}\,\rho_{\mathrm{tissue}}}\frac{1}{\tau}. \tag{3}$$

MW_{Hb} is the gram molecular weight of hemoglobin (64.5 kDa) and ρ_{tissue} is the density of brain tissue (=1.04 g/mL[30]). HGB is the hemoglobin content of blood and is assumed to be 16 gm/dL.[31]

At steady state, relative $CMRO_2$ is the product of blood flow [from Eq. (3)] and the oxygen extraction fraction across the vascular compartments. In the model, oxygen saturation values in each compartment are estimated parameters, which determine the relative magnitude and temporal dynamics of the evoked oxy-, deoxy-, and total-hemoglobin changes relative to blood flow. Thus, baseline $CMRO_2$ is calculated directly from the baseline blood flow and oxygen extraction (OE; $\mathrm{OE}=s_{\mathrm{in}}\mathrm{O}_2-s_{\mathrm{out}}\mathrm{O}_2$),

$$\mathrm{CMRO}_{2|0} = H_n\,\mathrm{HGB}\,\mathrm{CBF}_0\,\mathrm{OE}_0, \tag{4}$$

where H_n defines the oxygen carrying capacity of blood (H_n = 1.39 mL O_2/gm Hb[31]). Although the estimate of $CMRO_2$, blood flow, and volume in the conventional units mL/100 g (/min) requires the use of an estimate for the hemoglobin content of the blood, which may vary between animals, this factor cancels in the calculation of the fractional difference between the normal and hypercapnic states, allowing a direct comparison with measurements.

4 Results

Under both normal and hypercapnic conditions, we observed that the whisker deflection stimulation evoked increases in blood flow and volume and a decrease in the oxygen extraction fraction (decrease in deoxyhemoglobin and increase in oxyhemoglobin) typical of a "positive BOLD" response. As shown in Fig. 2 for the group average of the seven rats, the experimental results confirmed a trend between the amplitude of the whisker deflection and the magnitude of the experimentally measured evoked blood flow, hemoglobin, and electrophysiological signals. This linear trend was observed under both normal and hypercapnic conditions. A further comparison of the magnitudes of the evoked responses under the normal and hypercapnic states revealed that the hypercapnic responses were statistically lower in amplitude than the normal responses for all three hemoglobin variables; oxy-, deoxy-, and total-hemoglobin changes based on three-way ANOVA testing ($p<0.05$; see Table 2 using the individual rat and stimulus condition as the independent variables and the normal/hypercapnia condition as the dependent variable). In addition, the time-to-peak of the total-, oxy-, and deoxyhemodynamic responses were qualitatively observed to be earlier during hypercapnia, although this difference was not statistically significant by this same analysis. This empirical finding is consistent with similar observations made in previous rat model studies,[8] but is opposite from previous observations that the BOLD signal becomes slower in the human brain.[7]

Furthermore, we found that the peak magnitude of both the flow and hemoglobin responses were approximately linear

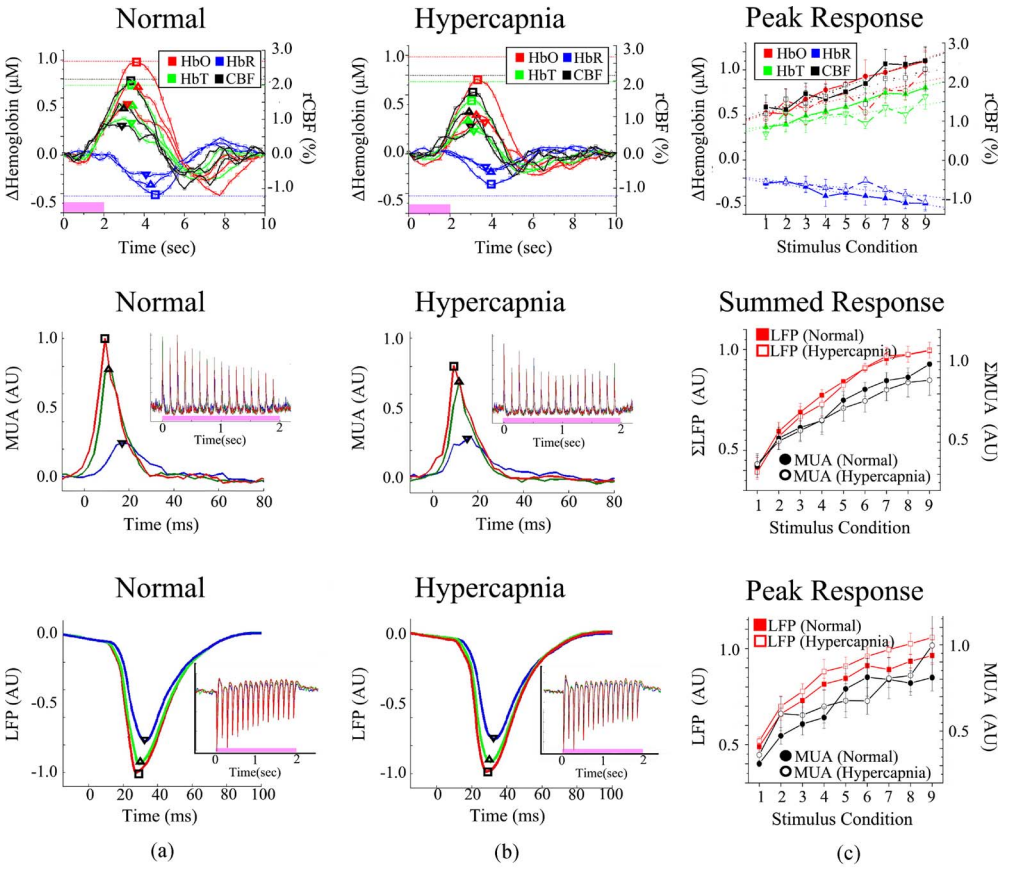

Fig. 2 Evoked hemodynamic and neuronal response. Columns (a) and (b) show the evoked hemodynamic changes, MUA, and LFP responses to whisker stimulation (conditions 3, 6, and 9) under normal and hypercapnic conditions. These responses show the ΔCBF, ΔHbO, ΔHbR, and ΔHbT (change) from baseline. Symbols are used to indicate condition 3 (▼), 6 (▲), and 9 (■) responses. The average MUA and LFP responses over the stimulus train are shown in rows 2 and 3. The response to stimulus conditions 3, 6, and 9 are shown in blue, green, and red, respectively, and are indicated by the neighboring text. The MUA and LFP responses are shown for the entire 2-sec stimulus train (inset figures) and response to a single deflection (averaged over train of responses). Column (c) shows the peak response amplitudes for the nine stimulus conditions. Open symbols indicate the hypercapnic data. The magnitudes of the LFP responses have been inverted for better visualization in column (c). Error bars indicate the standard deviation across the seven animals. The horizontal lines in (a) and (b) indicate the heights of the normal responses. (Color online only.)

with the amplitude of the stimulus deflection under both normal and hypercapnic conditions. We used a two degree of freedom linear model (slope and intercept) to describe this relationship. The linear goodness-of-fit (R^2) statistic between deflection magnitude and the experimentally measured peak response were determined to be 0.96*, 0.97*, 0.93*, and 0.97* for the flow, and oxy-, deoxy-, and total-hemoglobin response under normocapnia respectively (* indicates $p < 0.05$). The hypercapnic responses were generally less robust than the normocapnia responses, and the goodness-of-fit statistics for the linear model were 0.97**, 0.45*, 0.50*, and 0.43 for the flow, and oxy-, deoxy-, and total-hemoglobin response under hypercapnia, respectively.

In comparison to the evoked hemodynamic signals, no statistical differences in the average magnitudes of evoked local field potentials (Σ LFPs) or multiunit activity (Σ MUA) was observed between the normal and hypercapnic conditions (see Table 2). However, we did observe that the peak LFP response was significantly elevated under hypercapnia [see Fig. 2(c) and Table 2]. We found that, like the hemodynamic variables, the magnitudes of the LFP and MUA responses increased with stimulus condition. Both the peak and mean LFP responses followed an approximately linear relation to the stimulus condition under both normal and hypercapnia (for the peak response, $R^2=0.85$* for normocapnia and $R^2=0.88$* for hypercapnia; for the mean LFP response, $R^2=0.23$ for normocapnia and $R^2=0.55$* for hypercapnia; * indicates $p<0.05$). To further examine if this relationship was better described by a linear or nonlinear model, we also tested a nonlinear relationship between whisker deflection and response amplitudes [$f(x)=a\cdot x^b$ with two model degrees of freedom]. We found that only the peak LFP response could be statistically ($p<0.05$) better approximated with the nonlinear model in comparison to the linear model using a paired T-test of the Z-transformed R values (adjusted for degrees of freedom). In contrast to the LFP results, MUA and hemodynamic responses were not significantly improved by the nonlinear model and could be sufficiently modeled by the linear model. Note that this result indicates that any potential nonlinearity

Table 2 ANOVA comparisons of normal and hypercapnic response profiles. This table shows the probability of the null hypothesis testing for differences between normocapnia and hypercapnia in the response amplitudes of the hemodynamic and electrophysiological responses. The first two columns correspond to analysis performed on the raw measured signals. The latter columns refer to analysis of the amplitudes of the modeled responses, i.e., the fitted values of the hemoglobin responses. In the three-way ANOVA test, the response amplitude was the dependent variable, and the gas condition (df=1), stimulus condition (df=8), and animal (df=6) were the independent regressors. The two-way ANOVA test uses the group average and collapses across per individual animal degree of freedom. Note that the probability value can either increase or decrease between the three- to two-way ANOVA, depending on the contributions of inter- versus intrasubject variability. The values for the peak and Σ MUA (Σ LFP) responses refer to the maximum response amplitude for each response and the integrated area under the response curve, respectively.

	Individual animals three-way ANOVA	Group result two-way ANOVA
ΔHbO_2	0.006	0.012
ΔHbR	0.012	0.029
ΔHbT	0.005	<0.001
rCBF	0.233	0.001
$rCMRO_2$	0.984	0.717
MUA (peak)	0.271	0.289
Σ MUA	0.103	0.226
LFP (peak)	<0.001	0.007
Σ LFP	0.363	0.077

was not pronounced enough to significantly justify the higher order model, but that we cannot rule out the possibility of a nonlinear relationship by this analysis.

4.1 *Vascular and Metabolic Responses*

Once we had examined the correlations between the measured neural and hemodynamic signals, our multicompartment vascular model was used to further investigate the underlying neurovascular and neurometabolic changes by fitting the parametric hemodynamic and flow responses measured during normal and hypercapnic levels of cerebral perfusion (see Fig. 3). Our vascular model was simultaneously fit to the multimodal measurements (oxy/deoxyhemoglobin and blood flow) from all nine stimulus conditions (27 total time courses each characterized by at least two timing (e.g., peak and width) and one magnitude degree of freedom). The model was applied independently to the normal and hypercapnic states. By fitting the model to this data, we were provided with an estimate of the nine levels of evoked $CMRO_2$ and arterial resistance changes, as well as estimates of the biomechanical and baseline-related parameters for the normal and hypercapnic states. These results are shown in Table 3 for the group-averaged dataset. Since we considered the normal and hypercapnic responses independently, no restrictions are explicitly imposed about the relationships of parameters from the normal and hypercapnic estimates, for example, baseline flow was not necessarily assumed to be higher in the hypercapnic state. This provided a further physiological check on results of our model.

In Fig. 4, we show the timecourses of the estimated changes in arterial diameter and relative $CMRO_2$ changes. We note that the magnitudes of both of these states increased with stimulus condition, as did the hemodynamic measurements from which they were derived. In Fig. 4(b), we show the magnitude of peak response of the relative $CMRO_2$ changes estimated from the model for the normal and hypercapnic conditions. No statistical differences were noted for the magnitude of the relative $CMRO_2$ response under normal and hypercapnic conditions (see Table 2).

We found that the mean vascular transit time was slightly decreased under hypercapnia from 0.63 to 0.57 sec, although this difference was not statistically significant for the given level of uncertainty in the measurements. This is in agreement with the experimental observations that hypercapnic increases in flow are larger than volume changes. We also found that estimate of baseline total hemoglobin concentration also increased from 103 to 108 μM, and that the oxygen saturation levels of the three vascular compartments also increased (Table 4). Based on the values of the estimated model parameters and baseline physiology, we are able to determine the magnitudes of absolute blood flow and $CMRO_2$ changes. The parametric changes in absolute $CMRO_2$ and blood flow are shown in Fig. 4. We found no statistical differences in the parametric responses in absolute $CMRO_2$ changes between normal and hypercapnic states ($p>0.3$), see Table 2).

We found no significant difference in the magnitude of the absolute flow changes under normal and hypercapnic conditions [Fig. 3(b)], while there was a significant difference in the magnitude of the relative flow changes (Table 2). This is consistent with the results and discussions presented in Ref. 17. To further probe this, we examined the neurometabolic and neurovascular coupling relationship by correlating the values of the evoked $CMRO_2$ and blood flow signals predicted by our model with the magnitudes of the stimulus and experimentally measured neural signals. For this, we examined both the evoked relative and absolute changes in $CMRO_2$ and blood flow changes (see Sec. 4.2). Similar to the hemodynamic measurements, we found that both flow and $CMRO_2$ changes were approximately linear with the stimulus deflection amplitude. We noted that the goodness of fit for the linear model was $R^2=0.91^*$ (normal) and 0.70* (hypercapnia) for the $CMRO_2$, and $R^2=0.96^*$ (normal) and 0.97* (hypercapnia) for the flow changes (* indicates $p<0.05$).

We further examined the ratio of the evoked flow and consumption changes. We found that both the relative and absolute valued flow-consumption relationships could be fit using a linear model, which implies that the flow-consumption ratio did not significantly vary over the nine stimulus conditions within each gas state (normal or hypercapnia). The goodness-of-fit statistics for these linear fits were $R^2=0.72^*$ (normal) and 0.56* (hypercapnia) for the ratio of relative changes, and $R^2=0.88^*$ (normal) and 0.77* (hypercania) for the ratio of absolute changes (* indicates $p<0.05$). However, because the evoked relative blood flow response was statistically lower under hypercapnia but the oxygen consumption change

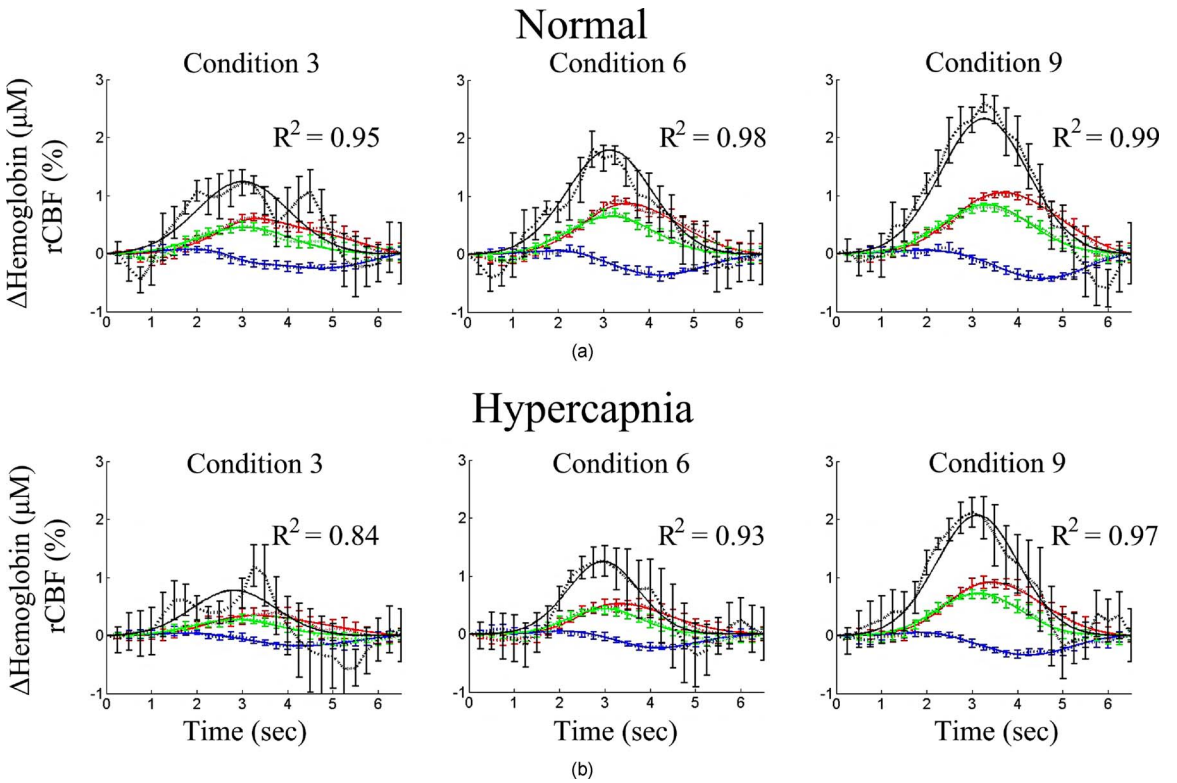

Fig. 3 Model fits of evoked hemodynamic changes. This figure shows the group-averaged hemodynamic responses (dotted lines; error bars indicate StdErr) under normal and hypercapnic conditions for stimulus conditions 3,6, and 9. The solid lines show the best fit of the model using these data points. Relative blood flow, oxyhemoglobin, deoxyhemoglobin, and total-hemoglobin changes are shown in black, red, blue, and green, respectively. The *R*-squared (goodness of fit) for the modeling of the full multimodal data is given above each plot. (Color online only.)

was not, the ratio of relative flow-to-consumption changes was also lower for the hypercapnic relationship ($p=0.03$). The statistical significance of this difference was tested through a two-way ANOVA analysis using the quotient of flow and consumption changes as the dependent variable, and CO_2 level and stimulus condition as the two independent variables. The flow-to-consumption ratio was not significantly different across stimulus conditions ($p>0.3$), which is consistent with the previous statement of linearity. This result implies that although flow and consumption changes were correlated across the stimulus conditions, there was an intrinsically different gain between normal and hypercapnic conditions. The ratio of the relative flow change to relative consumption change was 2.5:1 and 2.0:1 for the normal and hypercapnia responses, respectively. In comparison to the relative flow-to-consumption ratio, the ratio of absolute flow and absolute consumption was not statistically different between the normal and hypercapnic conditions ($p>0.4$, two-way ANOVA as previously described). These ratios were estimated to be 27:1 and 31:1 mL/100 g/min per mL O_2/100 g/min for the normal and hypercapnic conditions. This ratio was also not significantly different across the multiple stimulus conditions ($p>0.15$). This finding suggests that the ratio of absolute flow and absolute oxygen consumption is more robust to changes induced by hypercapnia. Note that this ratio of absolute changes is equivalent to normalization of both the normal and hypercapnic evoked responses to a common baseline state, whereas the report of relative flow and consumption changes is equivalent to independent normalization to the respective normal and hypercapnia level of baseline values. Unfortunately, the latter renormalization is a more realistic expectation for most experimental human neuroimaging studies, since we generally do not know the level of base-

Table 3 Estimated vascular parameters. The vascular model parameters related to the biomechanical and baseline properties of the vascular network were estimated from the nonlinear fit of the model to the experimental data. This table shows the values of the model parameters from the fit of the group-averaged responses from the seven animals.

Model parameter		Normal	Hypercapnia
Ra_o	%	79±4	79±2
Beta (β)	[AU]	1.5±0.7	2.0±0.1
Tau (τ)	seconds	0.60±0.55	0.57±0.19
Tau-pial	seconds	0.96±0.11	1.07±0.07
SaO_2	%	93.8±0.6	97.4±0.1
ScO_2	%	69.4±4.3	72.8±1.0
SvO_2	%	61.6±5.7	65±1.3

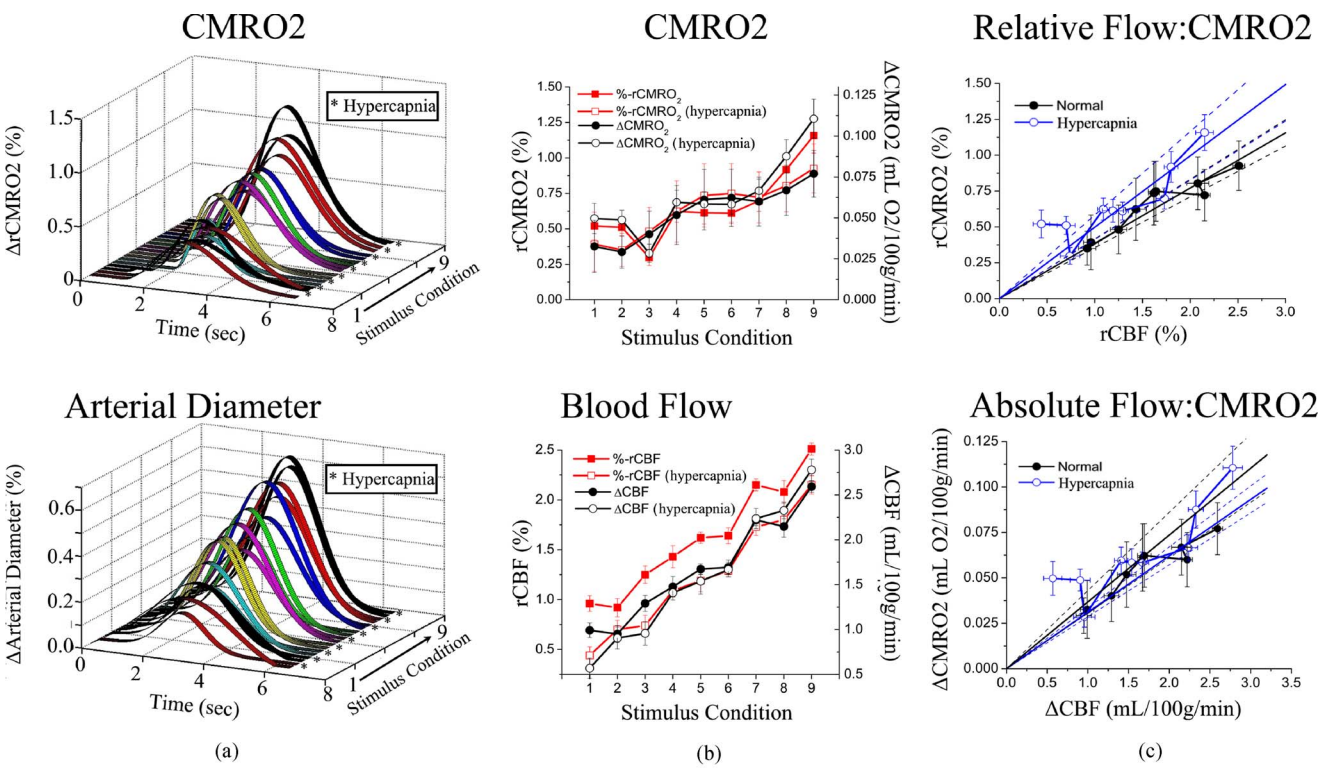

Fig. 4 Model estimates of arterial diameter and $CMRO_2$ changes. In column (a), the temporal dynamics of the evoked $CMRO_2$ (top row) and arterial diameter changes estimated by the model are plotted for the nine stimulus conditions (hypercapnic time courses are indicated with an asterisk). Column (b) shows the peak magnitude of $CMRO_2$ and CBF changes versus stimulus condition. The left-side axis (red lines) shows the relative CBF and $CMRO_2$ changes, whereas the right-side axis (black lines) shows the absolute changes. Column (c) shows parametric plots of the CBF versus $CMRO_2$ changes for comparison of the flow-consumption ratio. (Color online only.)

Table 4 Recovered baseline properties and measured hypercapnic changes. Values for the estimated model parameters were used to calculate the values for baseline total hemoglobin (THC), volume (CBV), flow (CBF), cerebral oxygen delivery (DO_2), oxygen extraction fraction (OEF), and $CMRO_2$ as described in the text. The percent difference between normal and hypercapnic states is also shown as the change from the normal state. For comparison, the hemodynamic changes measured during the hypercapnic transition are also shown (as described in the text). For calculations based on the measured changes, the superscript *a* indicates the assumption of a baseline total hemoglobin of 100 μM, and *b* indicates the assumption of a baseline oxygen extraction fraction of 37% (as described in text). * indicates significant differences ($p<0.05$).

		Results of model analysis			
		Normal	Hypercapnia	Difference	Measured change percent difference
THC	μM	103±3	108±2	4.5% *	3.2±0.2% *[a]
CBV	ml/100 g	2.5±0.1	2.6±0.1	4.5% *	—
CBF	ml/g/min	0.9±0.2	1.1±0.1	17.4%	9.0±1.8% *
DO_2	ml O_2/100 g/min	20.5±4.9	24.1±2.4	17.4%	—
OEF	%	37.2±2.0	34.0±0.4	−8.6% *	−5.6±1.9% *[a,b]
$CMRO_2$	ml O_2/100 g/min	7.7±2.2	8.3±0.9	8.0%	2.0±4.0% *[a,b]
MUA power		—	—	—	1.1±1.5%

line physiology and therefore cannot correct for baseline changes across longitudinal sessions.

4.2 *Baseline Physiology*

Using our model-based approach to examine the relative temporal properties of multimodal measurements, the estimated model parameters, in particular the baseline concentration of total hemoglobin, mean vascular transit time, and oxygen saturation levels can be related to estimates of baseline vascular and metabolic physiology as detailed in Refs. 21 and 28. Baseline total hemoglobin, which estimated the calibration factor between the normalized (fractional) changes estimated from the model on the basis of relative changes in blood flow and the relative magnitudes of the oxy- and deoxyhemoglobin changes, can be related to the value of baseline cerebral blood volume for a given value of the hemoglobin content of the blood (see Sec. 2). These baseline values were also used to renormalize the relative evoked signals to provide estimates of the absolute units of $CMRO_2$ and flow changes. The value of normal and hypercapnic levels of blood flow and volume allows the calculation of the changes evoked during the hypercapnic swing. Because these estimates are obtained from the dynamics of the evoked responses at each gas level, and makes no use of the data measured during the swing period, these estimates allow the model to be cross-validated by comparing these estimated values to the direct measurement of these changes.

In Table 4, we present the model estimated and experimentally measured changes in blood flow, volume, and $CMRO_2$ between normal and hypercapnia states. We found that cerebral blood volume increased from 2.5 to 2.6 ml/100 g, representing a $4.5 \pm 3.2\%$ increase (95% confidence bounds), which was comparable with the 3.2% experimentally measured increase in total hemoglobin content during the hypercapnia transition. The model-estimated blood flow increase during the hypercapnic transition was 17%. This was almost four-fold larger than the volume change. These flow and volume changes follow the previously proposed steady-state flow-volume relationship [$r\mathrm{CBV}=(r^{\mathrm{CBF}})^{1/(\alpha+\beta)}$ Grubb relationship[32]] with an exponent of $1/(\alpha+\beta)=0.27$. The measured blood flow change ($9.0 \pm 1.8\%$) was lower than the model estimated value, but within the range of the error bounds of the estimates. Using the measured values of flow and volume changes during the transition as given in Table 4, $1/(\alpha+\beta)=0.36 \pm 0.1$.

The optical measurements of oxy- and deoxyhemoglobin changes during the hypercapnic transition can also be used to estimate change in the relative oxygen extraction fraction and relative $CMRO_2$ in combination with the blood flow measurements. From both the direct measurements and the model-based analysis, we estimated that the oxygen extraction fraction decreased in the transition from normal to hypercapnia (see Table 4). In both of the model analysis and direct experimental measurements, this decrease was less than the fractional flow increase, which implies that $CMRO_2$ increased over this period. In both the model and direct measurement assessments, the elevation of $CMRO_2$ was observed but was not statistically significant. In addition, the measured root-mean-squared fluctuations (spectral power) of the MUA signal increased by approximately 1.1% under hypercapnia, but this was also not significant.

4.3 *Neuro-Metabolic-Vascular Coupling*

In comparison to the majority of previous studies that have been restricted to relative changes, the model-based assessment of both relative and absolute changes in oxygen metabolism, flow, and hemodynamic variables allows us to further investigate the relationships between evoked neuronal and hemodynamic changes. First, we note that in the case of the measured oxy- and deoxyhemoglobin responses, the normal and hypercapnic responses were significantly different from one another, although in both cases the response magnitudes were approximately linear with respect to the stimulus condition. In contrast, both MUA and LFP responses were fairly nonlinear with respect to the stimulus condition. More notably, however, there were no significant differences between the responses under normal and hypercapnic states for either evoked or baseline MUA. Thus, although a similar linear relationship was observed between oxy- and deoxyhemoglobin and the electrophysiological signals, the coupling constant was different for the normal compared to the hypercapnic responses (Fig. 5). The normal and hypercapnic relationship between the peak LPF response and oxy- and deoxyhemoglobin was significantly different using a two-way ANOVA test ($p<0.01$ and $p<0.02$ for HbO_2 and HbR, respectively; see Table 5). Furthermore, the linear coupling between the hemoglobin changes and the peak MUA responses were also significantly different between the normal and hypercapnic conditions ($p<0.001$ and $p<0.002$ for HbO_2 and HbR, respectively).

In contrast to the measured hemoglobin responses, which were significantly different between normal and hypercapnic conditions, the absolute flow change was unaltered by the hypercapnia (Table 2). In comparison, the relative blood flow responses (with the hypercapnic response renormalized to the elevated baseline) were significantly lower in the hypercapnia condition (Table 2). This suggests an additive model of the flow response to neuronal changes. We examined the coupling between these flow responses and the electrophysiological measurements and found significant differences in the coupling of relative versus absolute flow (Fig. 4). Although we observed that the relationships were qualitatively similar in all four combinations, we found that the coupling between relative flow and the integrated LFP responses was shifted between the normal and hypercapnic responses (Table 5). In comparison, the integrated LFP response and absolute flow coupling were not significantly altered under hypercapnia ($p>0.2$, two-way ANOVA). Similarly, we found that coupling between relative flow changes and integrated MUA to be different under normal versus hypercapnia ($p<0.007$). The MUA to absolute flow relationship was similar between these two conditions ($p<0.5$). We found that the coupling between LFP or MUA and flow was well approximated with a linear model ($R^2=0.83$ and 0.86 for LFP and MUA coupling under normal conditions, and $R^2=0.94$ and 0.94 respectively under hypercapnic conditions). The previously introduced nonlinear model ($a \cdot x/(b \cdot x)^c$) provided a slightly better fit than the linear model, but these differences were nonsignificant after adjusting for the additional degree of freedom (paired T-test on

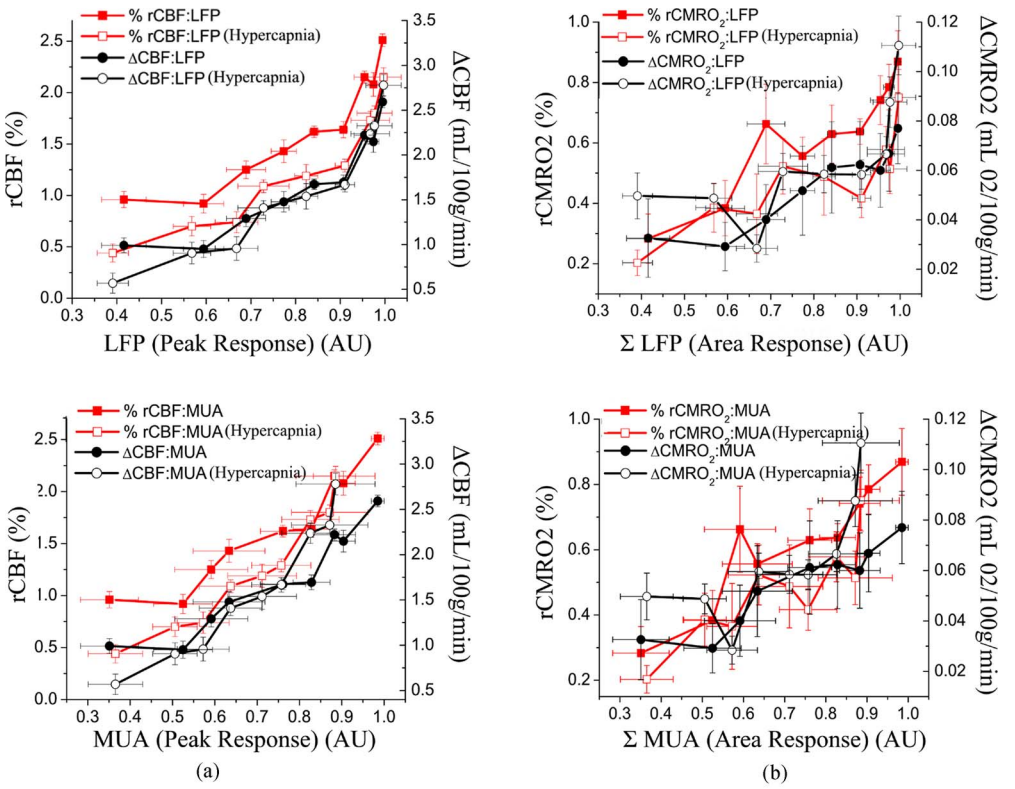

Fig. 5 Neuro-metabolic-vascular coupling. In this figure, we show the relationships between flow and metabolism changes and the electrophysiological measurements. In each panel, the relative change (flow or $CMRO_2$) is given on the left-side axis (red line). Absolute changes in flow and $CMRO_2$ (determined by renormalization to the baseline estimate as described in the text) are given by the right-side axis (black line). Hypercapnic responses are indicated with open symbols. ANOVA analysis of the differences between the normal and hypercapnic coupling is shown in Table 5. (Color online only.)

the Z-transformed R values).Finally, we examined the coupling between neuronal activity and oxygen metabolism ($CMRO_2$). There were no significant differences between the normal and hypercapnic metabolic responses (Table 5). Thus, the coupling between the LFP (or MUA) measurements and relative $CMRO_2$ and absolute $CMRO_2$ were similar and not significantly different. We found a significant linear relationship between LFP or MUA and relative $CMRO_2$ changes (R^2=0.93 and 0.84 for LFP and MUA coupling under normal conditions, and R^2=0.94 and 0.90 respectively under hypercapnic conditions). The coupling between the LFP and MUA responses and $CMRO_2$ were slightly better approximated with the nonlinear relationship than a simple linear relationship, but this improvement was not significant given the additional degree of freedom in the nonlinear model.

Finally, we compared the linear models of neurovascular and neurometabolic coupling to examine whether the intercepts of these relationships were significantly nonzero. We found that the flow-MUA and flow-LFP linear relationship had a significantly nonzero intercept, which would indicate that at small changes in neural activity, flow changes were not evoked, and indicates a minimum activation energy for the flow response. We note, however, that we cannot differentiate between a linear model with a nonzero intercept (piecewise linear model) and our nonlinear model that contains the zero-zero crossing. However, both of these models are significantly better than the slope-only (simple linear) model based on the fit to the data and degrees of freedom of the model (T-test of Z-transformed model fit metric; adjusted R-squared). In contrast to the neurovascular coupling, the intercept of the $CMRO_2$ and MUA or LFP responses was not significantly different from zero, which indicates that there was no significant minimum electrical threshold required to evoke a $CMRO_2$ change.

5 Discussion

Cerebral hemodynamic responses are the net result of a complex interplay of neurovascular and neurometabolic coupling. In part, the interpretation of measurements of blood oxygenation changes, such as the BOLD signal, is ambiguous because of the inability to separate the roles of metabolism and flow-inducing signals. This interpretation is additionally complicated by possible variability in the biomechanical properties of the vascular network. Mechanical properties of the vascular network, such as the mean vascular transit time, depend on the underlying vascular physiology. There is increasing evidence that variations in baseline cerebral blood flow, volume, or oxygen saturation can alter the magnitude and temporal characteristics of evoked blood oxygenation changes by changing these biomechanical properties.[7–10,17] In light of this observation, it is unclear the degree to which intersubject, interspecies, or spatial variability in such baseline physiology may affect the relationship between neuronal electrophysiol-

Table 5 ANOVA analysis of neurovascular coupling. This table shows the probability and result (as significant, yes or no) of the null hypothesis for a three-way ANOVA test for the differences between the normal and hypercapnic neurovascular coupling (plots shown in Fig. 5). The quotient of the amplitude of hemodynamic parameter (rows in table) and MUA or LFP value (quadrants of table) was the dependent variable, and the stimulus condition (df=8) and CO_2 level (df=1) were the independent variables.

	LFP response (peak)				ΣLEP response (area)			
	Relative response		Absolute response		Relative response		Absolute response	
ΔCBF	<0.001	***Yes***	0.032	***Yes***	0.001	***Yes***	0.248	***No***
$\Delta CMRO_2$	0.659	***No***	0.251	***No***	0.451	***No***	0.062	***No***
ΔArterial Diameter	<0.001	***Yes***	<0.001	***Yes***	0.002	***Yes***	0.002	***Yes***
ΔHbO_2	0.002	***Yes***	0.010	***Yes***	0.016	***Yes***	0.076	***No***
ΔHbR	0.020	***Yes***	0.018	***Yes***	0.145	***No***	0.102	***No***
ΔHbT	0.004	***Yes***	0.009	***Yes***	0.030	***Yes***	0.064	***No***
	MUA response (peak)				**ΣMUA response (area)**			
ΔCBF	0.004	***Yes***	0.105	***No***	0.007	***Yes***	0.527	***No***
$\Delta CMRO_2$	0.640	***No***	0.111	***No***	0.333	***No***	0.036	***Yes***
ΔArterial Diameter	0.001	***Yes***	0.001	***Yes***	0.004	***Yes***	0.004	***Yes***
ΔHbO_2	<0.001	***Yes***	0.001	***Yes***	0.014	***Yes***	0.088	***No***
ΔHbR	0.002	***Yes***	0.002	***Yes***	0.178	***No***	0.087	***No***
ΔHbT	0.001	***Yes***	0.003	***Yes***	0.033	***Yes***	0.077	***No***

ogy and blood oxygenation changes. Thus, to generalize the relationships between the neural, metabolic, vascular, and hemodynamic responses, it is necessary to account for the influences of variability in baseline physiology and vascular structure and biomechanics. The purpose of this work was to explore which of these variables change during hypercapnia, and furthermore, if these effects can be predicted from the baseline physiology using a vascular model.

In this work, we made several observations based on both our experimental results and the interpretation of the data using our vascular model-based approach. First, we experimentally confirmed previous observations that hypercapnia alters the amplitude and timing of blood oxygenation responses to a specific stimuli. Specifically, this was demonstrated with a parametric whisker deflection stimulation in rats. Second, we experimentally showed that under both normal and hypercapnia conditions, an approximately linear relationship was observed between underlying neural activity and blood flow, volume, oxy-, and deoxyhemoglobin changes. Using the model-based estimates, we found that oxygen metabolism changes were also linear with neural activity. We did not detect a difference between MUA and LFP. While this is in agreement with previous reports of linearity between neural and blood oxygenation changes (e.g., Ref. 16), we note that this may be explained by a first-order approximation of a more complex relationship, given the relatively small range of stimulus perturbations. Notably, however, the linear relationship between neural activity and oxy/deoxyhemoglobin (e.g., the slope of the line) changed when baseline physiology was perturbed. Conceptually, this can be explained by noting that since blood oxygenation changes are largely the result of washout effects, when baseline blood oxygen saturation (oxygen extraction fraction) is increased (decreased) due to baseline flow increases, then a similar blood flow change will produce a smaller evoked change in blood oxygenation (e.g., less washout effect since there was a smaller fraction of deoxyhemoglobin to start with). Related to this, our third conclusion was that our model could predict the effect of hypercapnia on the basis of how the model parameters, including baseline oxygen saturation, differed between normal and hypercapnic states. We found that the model parameters estimated from the separate normal and hypercapnia set of responses were consistent with the changes in blood flow measured during the hypercapnia transition. When we accounted for these baseline changes, we found that the blood flow and oxygen metabolism changes were additive to the effect of the hypercapnia. The absolute changes in blood flow and $CMRO_2$ (e.g., mL/100 g/min), rather than the normalized (percent) changes, were most closely coupled to the neural activity across the normal and hypercapnic conditions. This conclusion supports the earlier similar experimental findings by Sicard and Duong.[17] Finally, when we looked at the linear relationship between neural activity, flow, and $CMRO_2$,

we found that intercept of the neurovascular relationship was statistically nonzero, whereas the intercept was zero for the neurometabolic relationship. This suggested that a minimum electrical threshold is required to evoke a flow change, but that $CMRO_2$ is directly proportional to neural activity without a minimum activation level.

5.1 *Dependence of Hemodynamic Changes on Baseline Physiology*

Our vascular model allows us to account for the effects of changes in the vascular biomechanical properties and to estimate these properties based on the relations between multimodal data. Our analysis showed that while the magnitude of the evoked hemodynamic response was approximately linear with respect to small perturbations in neural activity under both normal and hypercapnic conditions, this coupling was context specific and different between normal and hyperemic states. These alterations in the evoked response were consistent with our model's prediction of the biomechanical effects expected from the changes in baseline flow, volume, and oxygen saturation, which resulted from the hypercapnic challenge and is consistent with the recent findings by in Ref. 33.

We found that the hemodynamic measurements of oxy- and deoxyhemoglobin were most sensitive to the hypercapnic perturbation and significantly differed between these two states. Our hemodynamic measurements showed that under hypercapnia, the evoked hemodynamic signals were diminished in amplitude and there was a trend toward an earlier time-to-peak of the response, although this trend was nonsignificant. The reduction in the time-to-peak of the rat whisker barrel response is consistent with the figures of oxy-, deoxy-, and total-hemoglobin shown in Ref. 8. This finding, although consistent with the prior expectation that the vascular transit time would decrease under hypercapnia since the increase in blood flow should be several fold larger than the blood volume change (e.g., Ref. 32), is in contrast to observations of latency in the BOLD signal.[7,10] This discrepancy might be explained by differences in the effective contributions of the vascular compartments to these different measurements, which depend on both anatomical differences in the fractions of artery and veins and on the differential measurement sensitivity of the optical and MRI techniques. This is an issue that should be examined in further studies.

In comparison to the hemodynamic responses, most of the electrophysiological measurements were not significantly altered under hypercapnia, except for the magnitude of the peak LFP, which increased under hypercapnia. This behavior of LFP is consistent with previously observed high sensitivity of inhibitory interneurons to physiological challenges such as hypoxia and stroke, probably due to their high baseline firing rate and high metabolism. Inhibitory interneurons are relatively rare (20% of cortical neurons), and therefore do not contribute significantly to MUA. However, their partial silencing due to hypercapnic challenge could enhance the synaptic response reflected by LFP. As a result, the neurohemodynamic coupling relationship was significantly different between normal and hypercapnic states. The increase in peak LFP, along with the decrease in the hemodynamic parameters, causes a greater emphasis of this difference. Larger changes in neuronal levels in response to hypercapnia have been observed in awake rats [34,35] and it may be possible that the unaltered neuronal levels in our experiment are related to the anesthetic. These results imply that the direct magnitude of the hemodynamic changes is not an absolute predictor of this neuronal activity, since it can be altered according to the baseline state. However, for small perturbations, the comparison of the hemodynamic response to parametric stimulus conditions may be less sensitive to this effect.

We found that the magnitude of the $CMRO_2$ change was a better predictor of the electrophysiological activity, since it was relatively unchanged under hypercapnia. We determined that baseline $CMRO_2$ was slightly elevated under hypercapnia, but that this was not a significant change in either the model or the direct measurements. Thus, the comparison of proportional versus absolute $CMRO_2$ changes yielded similar findings. Note that the slight elevation of baseline $CMRO_2$ would be expected of a diffusion-limited oxygen transport model, and may reflect a transient increase in the oxygen content of the surrounding tissue rather than a true increase in metabolism.

5.2 *Neurovascular-Metabolic Coupling*

Due to the baseline dependence of evoked hemodynamic changes, the generality of coupling between neuronal and hemodynamic changes (i.e., the BOLD signal) may vary according to baseline physiology.[8,17] This implies that while examples of local linearity between neuronal activity and the BOLD signal may exist for small perturbations (e.g., Ref. 16 and this study), this coupling constant may vary according to baseline physiology and will, in general, be nonlinear over a larger range of perturbations. Adding to this, the value of baseline cerebral blood flow varies considerably between brain regions,[36] which may affect the comparison of neural and blood oxygenation coupling between activation regions. In part, this idea has been demonstrated by Chiarelli and coworkers et al.[37] in their recent comparison of studies using hypercapnia to calibrate the relationship between deoxyhemoglobin washout (BOLD) and blood flow changes (e.g., Ref. 38). Chiarelli et al. found that the BOLD-flow calibration factor (denoted M in many studies; e.g., Ref. 39) varied between brain regions, and hypothesized that this reflected underlying variations in vascular architecture and physiology. This result was intuitively expected, since the magnitude of washout of deoxyhemoglobin for a given change in blood flow will depend on the baseline value of blood oxygen saturation and venous volume fraction in that brain region.

Considering the potential baseline and biomechanical influences on the magnitude and temporal dynamics of evoked hemodynamic signals, in this work we examined the relationships between MUA and LFP measures of neuronal activity and the evoked hemodynamic and metabolic responses. Our analysis of evoked blood flow changes suggested that the magnitude of relative flow changes (i.e., renormalized to the normal or hypercapnic baseline value) were significantly decreased under hypercapnia. However, the absolute flow changes (both evoked changes normalized to the same prehypercapnia baseline value) were not significantly different. This result supports the surprising finding that functionally evoked flow changes are additive rather than proportional. This result is consistent with the earlier findings by Sicard and

Duong,[17] who reported that evoked absolute flow changes were similar under multiple levels of hypercapnia and hypoxia, but that the renormalized relative flow changes were significantly different. We have additionally shown that the evoked electrophysiological signals were also conserved across hypercapnia, and thus absolute flow changes are a better predictor of electrophysiology than relative flow. As a consequence of the differences in the relative flow changes between normal and hypercapnia, we found that the relative flow-to-consumption ratio was decreased under hypercapnia, but that the absolute flow-to-consumption ratio was not.

Although the LFP responses were significantly nonlinear with the stimulus condition, while the hemodynamic measures were linear, we did not statistically confirm that a nonlinear model was more significant than a linear model. We were unable to show that the linear coupling model was not sufficient. That is, that the improvements of the fit of the nonlinear model (i.e., Ref. 12) justified the additional degree of freedom. Note, however, that this result depends on whether the linear model contains only the slope or the slope and intercept degrees of freedom. For the neurovascular coupling, both the nonlinear model and the slope/intercept linear model provided a better fit than the slope-only model. In the linear model, the intercept of the flow verses LFP or MUA amplitudes was significantly nonzero for both the normal and hypercapnia conditions ($p < 0.05$, T-test for significance in the regression variable). All neurovascular comparisons were significant except for those between ΣLFP and flow under normocapnia only. This suggests that either there is nonlinear neurovascular or neurometabolic coupling or that that a minimum threshold electrophysiological change is needed to evoke a vascular change. However, because of the similarity of the goodness-of-fit statistics in these models, we cannot determine whether the nonlinear or the linear (slope/intercept) model is better than the other.

Based on our results, we hypothesized that there was no significant minimum electrical threshold required to evoke a $CMRO_2$ change, but a minimum level of neural activity appeared to be required to evoke a flow change. This result suggests that $CMRO_2$ is closely related to the underlying overall neuronal activity, whereas the induction of a flow change is an active process triggered by reaching a minimum neuronal or biochemical signal. This also suggests that neurometabolic and neurovascular coupling are distinct pathways in contrast to a model of diffusion-limited oxygen transport to the tissue.

The results of this work suggest that the coupling between neural activity, blood flow, and $CMRO_2$ is an intrinsic property of the brain and does not change due to mild changes in baseline physiology. Although much of the underlying processes remain unknown, we can appreciate that interactions between neurons and blood vessels occur at a biochemical level. While the mechanical response of the vascular system depends on baseline flow, volume, and oxygen extraction and this gives rise to the changes in evoked optical and fMRI signals, the underlying biochemistry of the neurovascular interaction driving these changes appears to be more robust to baseline effects. Likewise, one would hypothesize that factors that affect this biochemistry such as disease, age, genetics, etc. might manifest as changes in neurovascular and/or neurometabolic coupling. It is probable that this coupling also varies depending on the task and brain region, such that the neurovascular coupling "constant" is a value specific to a given individual and a given stimulus type reflecting the underlying biochemistry of a particular brain region. This could explain the recent work by Leontiev and Buxton,[40] where in repeated measurements over several days in the same subject, the flow-consumption ratio estimated by calibrated BOLD fMRI was more reproducible than the BOLD or $CMRO_2$ responses alone. In comparison, when they looked at the responses across different subjects, the flow-consumption ratio was more variable than the BOLD signal. This would suggest that neurovascular and neurometabolic coupling might be potential biomarkers for longitudinal studies of changes in an individual's brain.

6 Conclusions

Hemodynamic-based measurements such as the BOLD signal or optical measures of oxy- and deoxyhemoglobin are less informative of underlying neuronal activity than metabolism and blood flow changes, since the evoked hemodynamic signal is sensitive to variations in the baseline physiology of the brain. We find that hypercapnia-induced hyperemia significantly alter the neurohemodynamic coupling but the neurometabolic and neurovascular couplings remain unchanged. The dynamics and magnitudes of evoked oxygen washout changes depend on baseline flow, volume, and oxygen metabolism levels. Thus, we find that the underlying $CMRO_2$ and flow changes are more reliable indicators of neuronal activity compared to blood oxygenation measurements.

Acknowledgments

This work was supported by the National Institutes of Health (R01-EB002482, RO1-EB000790, R01-NS051188, and P41-RR14075), NCRR, and the MIND institute. The authors would like to thank Heval Benav and Rickson Mesquita, and Monica Allen, Solomon Diamond, Joe Mandeville, and Bruce Rosen for their roles in the development of this model and for helpful discussion on this manuscript.

References

1. M. Jones, J. Berwick, and J. Mayhew, "Changes in blood flow, oxygenation, and volume following extended stimulation of rodent barrel cortex," *Neuroimage* **15**(3), 474–487 (2002).
2. A. K. Dunn, A. Devor, H. Bolay, M. L. Andermann, M. A. Moskowitz, A. M. Dale, and D. A. Boas, "Simultaneous imaging of total cerebral hemoglobin concentration, oxygenation, and blood flow during functional activation," *Opt. Lett.* **28**(1), 28–30 (2003).
3. A. Grinvald, R. D. Frostig, R. M. Siegel, and E. Bartfeld, "High-resolution optical imaging of functional brain architecture in the awake monkey," *Proc. Natl. Acad. Sci. U.S.A.* **88**(24), 11559–11563 (1991).
4. A. J. Blood and A. W. Toga, "Optical intrinsic signal imaging responses are modulated in rodent somatosensory cortex during simultaneous whisker and forelimb stimulation," *J. Cereb. Blood Flow Metab.* **18**(9), 968–977 (1998).
5. S. Ogawa, T. M. Lee, A. R. Kay, and D. W. Tank, "Brain magnetic resonance imaging with contrast dependent on blood oxygenation," *Proc. Natl. Acad. Sci. U.S.A.* **87**(24), 9868–9872 (1990).
6. K. K. Kwong, J. W. Belliveau, D. A. Chesler, I. E. Goldberg, R. M. Weisskoff, B. P. Poncelet, D. N. Kennedy, B. E. Hoppel, M. S. Cohen, R. Turner, H.-M. Cheng, T. J. Brady, and B. R. Rosen, "Dynamic magnetic resonance imaging of human brain activity during primary sensory stimulation," *Proc. Natl. Acad. Sci. U.S.A.* **89**(12),

5675–5679 (1992).
7. E. R. Cohen, K. Ugurbil, and S. G. Kim, "Effect of basal conditions on the magnitude and dynamics of the blood oxygenation level-dependent fMRI response," *J. Cereb. Blood Flow Metab.* **22**(9), 1042–1053 (2002).
8. M. Jones, J. Berwick, N. Hewson-Stoate, C. Gias, and J. Mayhew, "The effect of hypercapnia on the neural and hemodynamic responses to somatosensory stimulation," *Neuroimage* **27**(3), 609–623 (2005).
9. Y. Behzadi and T. T. Liu, "Caffeine reduces the initial dip in the visual BOLD response at 3 T," *Neuroimage* **32**(1), 9–15 (2006).
10. T. T. Liu, Y. Behzadi, K. Restom, K. Uludag, K. Lu, G. T. Buracas, D. J. Dubowitz, and R. B. Buxton, "Caffeine alters the temporal dynamics of the visual BOLD response," *Neuroimage* **23**(4), 1402–1413 (2004).
11. G. G. Brown, L. T. Eyler Zorrilla, B. Georgy, S. S. Kindermann, E. C. Wong, and R. B. Buxton, "BOLD and perfusion response to finger-thumb apposition after acetazolamide administration: differential relationship to global perfusion," *J. Cereb. Blood Flow Metab.* **23**(7), 829–837 (2003).
12. A. Devor, A. K. Dunn, M. L. Andermann, I. Ulbert, D. A. Boas, and A. M. Dale, "Coupling of total hemoglobin concentration, oxygenation, and neural activity in rat somatosensory cortex," *Neuron* **39**(2), 353–359 (2003).
13. A. Devor, I. Ulbert, A. K. Dunn, S. N. Narayanan, S. R. Jones, M. L. Andermann, D. A. Boas, and A. M. Dale, "Coupling of the cortical hemodynamic response to cortical and thalamic neuronal activity," *Proc. Natl. Acad. Sci. U.S.A.* **102**(10), 3822–3827 (2005).
14. D. J. Heeger, A. C. Huk, W. S. Geisler, and D. G. Albrecht, "Spikes versus BOLD: what does neuroimaging tell us about neuronal activity?," *Nat. Neurosci.* **3**(7), 631–633 (2000).
15. N. K. Logothetis, "The neural basis of the blood-oxygen-level-dependent functional magnetic resonance imaging signal," *Philos. Trans. R. Soc. London, Ser. B* **357**(1424), 1003–1037 (2002).
16. N. K. Logothetis, J. Pauls, M. Augath, T. Trinath, and A. Oeltermann, "Neurophysiological investigation of the basis of the fMRI signal," *Nature (London)* **412**(6843), 150–157 (2001).
17. K. M. Sicard and T. Q. Duong, "Effects of hypoxia, hyperoxia, and hypercapnia on baseline and stimulus-evoked BOLD, CBF, and CMRO2 in spontaneously breathing animals," *Neuroimage* **25**(3), 850–858 (2005).
18. D. J. Heeger and D. Ress, "What does fMRI tell us about neuronal activity?," *Nat. Rev. Neurosci.* **3**(2), 142–151 (2002).
19. N. K. Logothetis and J. Pfeuffer, "On the nature of the BOLD fMRI contrast mechanism," *Magn. Reson. Imaging* **22**(10), 1517–1531 (2004).
20. R. B. Buxton, K. Uludag, D. J. Dubowitz, and T. T. Liu, "Modeling the hemodynamic response to brain activation," *Neuroimage* **23**(Suppl 1), S220–233 (2004).
21. T. J. Huppert, M. S. Allen, H. Benav, P. Jones, and D. A. Boas, "A multi-compartment vascular model for inferring arteriole dilation and cerebral metabolic changes during functional activation," *J. Cereb. Blood Flow Metab.* **27**, 1262–1279 (2007).
22. A. M. Dale, "Optimal experimental design for event-related fMRI," *Hum. Brain Mapp* **8**(2–3), 109–114 (1999).
23. A. K. Dunn, A. Devor, A. M. Dale, and D. A. Boas, "Spatial extent of oxygen metabolism and hemodynamic changes during functional activation of the rat somatosensory cortex," *Neuroimage* **27**(2), 279–290 (2005).
24. M. Kohl, U. Lindauer, G. Royl, M. Kuhl, L. Gold, A. Villringer, and U. Dirnagl, "Physical model for the spectroscopic analysis of cortical intrinsic optical signals," *Phys. Med. Biol.* **45**(12), 3749–3764 (2000).
25. J. D. Briers, "Laser Doppler, speckle and related techniques for blood perfusion mapping and imaging," *Physiol. Meas* **22**(4), R35–66 (2001).
26. A. K. Dunn, H. Bolay, M. A. Moskowitz, and D. A. Boas, "Dynamic imaging of cerebral blood flow using laser speckle," *J. Cereb. Blood Flow Metab.* **21**(3), 195–201 (2001).
27. I. Ulbert, G. Karmos, G. Heit, and E. Halgren, "Early discrimination of coherent versus incoherent motion by multiunit and synaptic activity in human putative MT+," *Hum. Brain Mapp* **13**(4), 226–238 (2001).
28. T. J. Huppert, "The hemodynamic inference of cerebral oxygen metabolism," in *Graduate Programs in Biophysics*, p. 503, Harvard University, PhD Thesis, Boston, MA (2007).
29. D. W. Marquardt, "An algorithm for least-squares estimation of nonlinear parameters," *J. Soc. Ind. Appl. Math.* **11**(2), 431–441 (1963).
30. G. R. DiResta, J. B. Lee, and E. Arbit, "Measurement of brain tissue specific gravity using pycnometry," *J. Neurosci. Methods* **39**(3), 245–251 (1991).
31. O. P. Habler and K. F. Messmer, "The physiology of oxygen transport," *Transfus. Sci.* **18**(3), 425–435 (1997).
32. R. L. Grubb, Jr., M. E. Raichle, J. O. Eichling, and M. M. Ter-Pogossian, "The effects of changes in PaCO2 on cerebral blood volume, blood flow, and vascular mean transit time," *Stroke* **5**(5), 630–639 (1974).
33. A. L. Vazquez, E. R. Cohen, V. Gulani, L. Hernandez-Garcia, Y. Zheng, G. R. Lee, S. G. Kim, J. B. Grotberg, and D. C. Noll, "Vascular dynamics and BOLD fMRI: CBF level effects and analysis considerations," *Neuroimage* **32**(4), 1642–1655 (2006).
34. C. Martin, M. Jones, J. Martindale and J. Mayhew, "Haemodynamic and neural responses to hypercapnia in the awake rat," *Eur. J. Neurosci.* **24**(9), 2601–2610 (2006).
35. C. Martin, J. Martindale, J. Berwick, and J. Mayhew, "Investigating neural-hemodynamic coupling and the hemodynamic response function in the awake rat," *Neuroimage* **32**(1), 33–48 (2006).
36. M. E. Raichle, A. M. MacLeod, A. Z. Snyder, W. J. Powers, D. A. Gusnard, and G. L. Shulman, "A default mode of brain function," *Proc. Natl. Acad. Sci. U.S.A.* **98**(2), 676–682 (2001).
37. P. A. Chiarelli, D. P. Bulte, S. Piechnik, and P. Jezzard, "Sources of systematic bias in hypercapnia-calibrated functional MRI estimation of oxygen metabolism," *Neuroimage* **34**(1), 35–43 (2007).
38. T. L. Davis, K. K. Kwong, R. M. Weisskoff, and B. R. Rosen, "Calibrated functional MRI: mapping the dynamics of oxidative metabolism," *Proc. Natl. Acad. Sci. U.S.A.* **95**(4), 1834–1839 (1998).
39. R. D. Hoge, J. Atkinson, B. Gill, G. R. Crelier, S. Marrett, and G. B. Pike, "Linear coupling between cerebral blood flow and oxygen consumption in activated human cortex," *Proc. Natl. Acad. Sci. U.S.A.* **96**(16), 9403–9408 (1999).
40. O. Leontiev and R. B. Buxton, "Reproducibility of BOLD, perfusion, and CMRO(2) measurements with calibrated-BOLD fMRI," *Neuroimage* **35**, 175–184 (2007).
41. D. A. Boas, G. Strangman, J. P. Culver, R. D. Hoge, G. Jasdzewski, R. A. Poldrack, B. R. Rosen, and J. B. Mandeville, "Can the cerebral metabolic rate of oxygen be estimated with near-infrared spectroscopy?," *Phys. Med. Biol.* **48**(15), 2405–2418 (2003).
42. J. B. Mandeville, J. J. Marota, C. Ayata, G. Zaharchuk, M. A. Moskowitz, B. R. Rosen, and R. M. Weisskoff, "Evidence of a cerebrovascular postarteriole windkessel with delayed compliance," *J. Cereb. Blood Flow Metab.* **19**(6), 679–689 (1999).
43. M. Ibaraki, H. Ito, E. Shimosegawa, H. Toyoshima, K. Ishigame, K. Takahashi, I. Kanno, and S. Miura, "Cerebral vascular mean transit time in healthy humans: a comparative study with PET and dynamic susceptibility contrast-enhanced MRI," *J. Cereb. Blood Flow Metab.* **27**, 404–413 (2006).
44. A. Torricelli, A. Pifferi, P. Taroni, E. Giambattistelli, and R. Cubeddu, "*In vivo* optical characterization of human tissues from 610 to 1010 nm by time-resolved reflectance spectroscopy," *Phys. Med. Biol.* **46**(8), 2227–2237 (2001).
45. P. Herman, H. K. Trubel, and F. Hyder, "A multiparametric assessment of oxygen efflux from the brain," *J. Cereb. Blood Flow Metab.* **26**(1), 79–91 (2006).